Invariant natural killer T cells act as an extravascular cytotoxic barrier for joint-invading Lyme *Borrelia*

Woo-Yong Lee[a,b,1], Maria-Jesus Sanz[c,d,1], Connie H. Y. Wong[a,b], Pierre-Olivier Hardy[a,e], Aydan Salman-Dilgimen[a,f], Tara J. Moriarty[a,f,2], George Chaconas[a,e,f], Adriana Marques[g], Roman Krawetz[h,i], Christopher H. Mody[a,e,j], and Paul Kubes[a,b,3]

[b]Department of Physiology and Pharmacology, [e]Department of Microbiology and Infectious Diseases, [f]Department of Biochemistry and Molecular Biology, [h]Department of Surgery, [i]Department of Cell Biology and Anatomy, [j]Department of Internal Medicine, and [a]Calvin, Phoebe, and Joan Snyder Institute for Chronic Diseases, University of Calgary, Calgary, AB, Canada T2N 4N1; [c]Department of Pharmacology, Faculty of Medicine, and [d]Institute of Health Research, INCLIVA, University of Valencia, E46010 Valencia, Spain; and [g]Clinical Studies Unit, Laboratory of Clinical Infectious Diseases, National Institute of Allergy and Infectious Diseases, National Institutes of Health, Bethesda, MD 20892

Edited by Michael L. Dustin, Kennedy Institute of Rheumatology, Headington, United Kingdom, and accepted by the Editorial Board August 13, 2014 (received for review March 17, 2014)

CXCR6-GFP$^+$ cells, which encompass 70% invariant natural killer T cells (iNKT cells), have been found primarily patrolling inside blood vessels in the liver. Although the iNKT cells fail to interact with live pathogens, they do respond to bacterial glycolipids presented by CD1d on liver macrophage that have caught the microbe. In contrast, in this study using dual laser multichannel spinning-disk intravital microscopy of joints, the CXCR6-GFP, which also made up 60–70% iNKT cells, were not found in the vasculature but rather closely apposed to and surrounding the outside of blood vessels, and to a lesser extent throughout the extravascular space. These iNKT cells also differed in behavior, responding rapidly and directly to joint-homing pathogens like *Borrelia burgdorferi*, which causes Lyme disease. These iNKT cells interacted with *B. burgdorferi* at the vessel wall and disrupted dissemination attempts by these microbes into joints. Successful penetrance of *B. burgdorferi* out of the vasculature and into the joint tissue was met by a lethal attack by extravascular iNKT cells through a granzyme-dependent pathway, an observation also made in vitro for iNKT cells from joint but not liver or spleen. These results suggest a novel, critical extravascular iNKT cell immune surveillance in joints that functions as a cytotoxic barrier and explains a large increase in pathogen burden of *B. burgdorferi* in the joint of iNKT cell-deficient mice, and perhaps the greater susceptibility of humans to this pathogen because of fewer iNKT cells in human joints.

joint iNKT cells | granzyme B | Lyme arthritis

An essential component of homeostasis is the delivery of oxygen and nutrients to tissues via an extensive vascular network. This process, however, also creates a portal for pathogens to exploit the dissemination of invading bacteria. Intravascular immunity is an emerging concept that suggests that the host immune system remain vigilant and proactive within the vasculature, limiting or preventing pathogen dissemination (1). As such, it is not surprising that numerous cell types have been discovered patrolling the vasculature, including rolling neutrophils in places like skin, crawling monocytes (2), and invariant natural killer T cells (iNKT cells) (3) in skin, brain, muscle, and lung, and immobilized macrophages, including Kupffer cells and splenic macrophage in liver and spleen, respectively (4). Although macrophage have been demonstrated to directly catch, phagocytose, and destroy various pathogens, iNKT cells have to date been suggested to receive signals via antigen presentation and produce potent cytokines that can enhance immunity to infections (4–6), but their direct role in killing pathogens has not been reported. However, it is worth mentioning a recent publication suggesting that iNKT cells can produce granzyme B (7), a molecule known to be used by other immune cells to kill tumor cells as well as various fungi.

The natural killer T cells, a subpopulation of T lymphocytes, express a T-cell receptor (TCR) with an invariant variable α-segment 14-joining α-segment 18 (Vα14-Jα18) TCR-α chain that is paired with a restricted subset of TCR Vβ chains in mice (Vα24-Jα18 or Vβ11 in humans) (5, 6). This highly restricted repertoire of TCRs expressed by iNKT cells allows them to recognize lipid antigens presented by CD1d (8, 9), a nonclassical MHC class I-like molecule. The most potent iNKT antigen identified was α-galactosylceramide (αGC) (10), and in vivo administration of this molecule leads to rapid stopping of patrolling iNKT cells with subsequent production of various cytokines, including IL-4 and IFN-γ (5, 6). More recently, several lipid antigens from pathogens have been reported, including α-galactosyl diacylglycerolipid from *Borrelia burgdorferi*, a spirochete responsible for human Lyme disease (8, 9, 11–13). Imaging of the intravascular immune response in vivo to αGC, which would exclusively bind CD1d, has shown a cessation of iNKT cell crawling and the production of cytokines. Unlike a specific CD1d ligand, an intact pathogen has many activating molecules, ranging from Toll-like receptor (TLR) ligands to complement to chemoattractants, and its direct interaction with iNKT cells is not fully elucidated.

B. burgdorferi is arguably the prototype emerging pathogen, becoming a global public health concern estimated at as many as 300,000 patients a year in North America (www.cdc.gov/media/releases/2013/p0819-lyme-disease.html). Lyme disease is one of

Significance

Invariant natural killer T cells (iNKT) have been found primarily patrolling inside blood vessels in the liver, where they respond to bacterial glycolipids presented by CD1d on liver macrophages. We show joint iNKT cells are localized outside of blood vessels and respond directly to the joint-homing pathogen, *Borrelia burgdorferi*, which causes Lyme borreliosis using multichannel spinning-disk intravital microscopy. These iNKT cells interacted with *B. burgdorferi* at the vessel wall and disrupted its dissemination attempts into joints. Successful penetrance of *B. burgdorferi* out of the vasculature and into the joint tissue was met by a lethal attack by extravascular iNKT cells through a granzyme-dependent pathway. These results suggest a critical extravascular iNKT cell immune surveillance in joints that functions as a cytotoxic barrier.

Author contributions: W.-Y.L., M.-J.S., G.C., C.H.M., and P.K. designed research; W.-Y.L., M.-J.S., C.H.Y.W., P.-O.H., A.S.-D., T.J.M., A.M., and R.K. performed research; W.-Y.L., M.-J.S., and C.H.Y.W. analyzed data; and W.-Y.L., M.-J.S., and P.K. wrote the paper.

The authors declare no conflict of interest.

This article is a PNAS Direct Submission. M.L.D. is a Guest Editor invited by the Editorial Board.

[1]W.-Y.L. and M.-J.S. contributed equally to this work.

[2]Present address: Matrix Dynamics Group, Faculty of Dentistry, and Department of Laboratory Medicine and Pathobiology, Faculty of Medicine, University of Toronto, ON, Canada M5S 3E2.

[3]To whom correspondence should be addressed. Email: pkubes@ucalgary.ca.

This article contains supporting information online at www.pnas.org/lookup/suppl/doi:10.1073/pnas.1404769111/-/DCSupplemental.

the most common vector-borne diseases and the number of infected patients is continuing to increase (14). A variety of symptoms have been identified, the most common late-stage manifestation being joint inflammation, known as Lyme arthritis (14). In most cases, treatment with antibiotics leads to resolution of symptoms, but in the absence of antibiotic therapy, intermittent or chronic synovial inflammation can occur (14, 15). Although iNKT cells have not been reported in joints of mice, mice lacking iNKT cells have a joint-specific 25-fold increase (PCR product) in pathogen burden in Lyme borreliosis (4, 13). Although it is well appreciated that iNKT cells receive signals from antigen-presenting cells to induce a systemic increase in IFN-γ, an important cytokine in the fight against infection, it is unclear why the absence of this response would favor localization of *B. burgdorferi* only in joints (4, 13). We hypothesized that the iNKT cells were also exerting their protective effects directly in the knee microvasculature. Indeed, we have identified a population of CXCR6-GFP$^+$ cells, 60–70% of which were iNKT cells that resided in the tissues and preferentially surrounding the joint vasculature. These cells performed direct immune surveillance in joints that function as a cytotoxic barrier, killing pathogens via a granzyme-dependent mechanism. These cells appear to be less prevalent in human joints and may explain the greater susceptibility to Lyme borreliosis in these human tissues.

Results and Discussion

Detection and Visualization of Knee Joint iNKT Cells in Mice and Humans. iNKT cells have been found to be most abundant in the liver, accounting for close to 30% of all immune cells in this organ (16), with significant numbers in the spleen, lung, and lymph nodes. Recently, a human study reported iNKT cells in knee joints of *B. burgdorferi*-infected patients (17), but their potential role was unknown. However, when we administered *B. burgdorferi* to iNKT cell-deficient mice, they had a 25-fold increase in pathogen tropism to joints compared with wild-type mice (using PCR), which have almost undetectable levels of this pathogen. Meanwhile, the liver and other organs show very minor changes in pathogen burden. In fact, the joint is the only organ to be significantly affected by iNKT cell deficiency. We visualized and compared the distribution of iNKT cells in the liver and knee joint of CXCR6-GFP mice, in which 60–70% of GFP$^+$ cells are iNKT cells (3, 4). In the liver, iNKT cells resided exclusively in the sinusoids (Fig. 1*A*) and crawled in a random pattern, at times changing directions 180°, as previously described by us and others (3, 4). On occasion the cells are swept away by the blood flow (Movie S1). In contrast, knee joint iNKT cells were not seen in the vasculature but rather were distributed throughout the extravascular tissue, with frequent prevalence surrounding blood vessels and remaining in close, if not intimate contact, with the microvasculature (Fig. 1 *B* and *C*). The iNKT cells were not uniformly distributed but rather were found predominantly at the surface of the knee joint (near the capsule and patella tendon, where bacteria appeared to adhere, as shown later), with only a few iNKT cells detected in the tissue located underneath (Fig. 1*C*). Unlike in the liver sinusoids, where most of iNKT cells crawl, 90% of iNKT cells in the joints were stationary (<2.5 μm/min) and less than 10% were seen to be slowly crawling almost exclusively near the vasculature (Fig. 1*D* and Movie S2).

Although surgery can always be a confounding variable in imaging, leading to this type of iNKT cell recruitment, it should be noted that we never saw recruitment of iNKT cells from the vasculature (they were already there). Despite the fact that surgical preparation of the joint was very minor and lasted less than 5 min, the iNKT cells were already outside the vasculature and not adhering in the vasculature, suggesting these were resident extravascular iNKT cells. Killing the mouse and fixing tissue before exposing the joint vasculature still revealed iNKT cells outside not inside the blood vessels. The extravascular location of these iNKT cells is further highlighted by 3D reconstructions (Movie S3). The nonpatrolling-stopped phenotype of the iNKT cells was evident despite no evidence of any inflammation: the joints and vessel were devoid of adhering and emigrating neutrophils, a hallmark feature of inflammation. Using either LysM-EGFP mice (fluorescent monocytes and neutrophils) or anti-mouse Ly-6G in wild-type mice (fluorescent neutrophils), we only saw rolling neutrophils with no neutrophils or monocytes adhering in the joint vessels, suggesting minimal activation of the preparations (Movie S4).

Not all CXCR6-GFP$^+$ cells are iNKT cells. The CXCR6-GFP cells that are not iNKT cells have been shown to be other small subpopulations of T cells (accounting for about 30%). When transgenic mice with CXCR6-GFP cells were crossed to Vα14-Jα18 TCR-transgenic mice (which have primarily iNKT cells at the expense of other T cells) and were examined using spinning-disk microscopy, imaging revealed similar distribution and amount of CXCR6$^+$ cells around joint vessels, again confirming a large proportion of these cells are iNKT cells (Fig. 1*E*). Fig. 1*F* shows the 3D reconstruction, highlighting the iNKT cells in the extravascular space, and Fig. 1*G* demonstrates that the majority of these iNKT cells are stationary.

Using a new immunohistochemical approach in whole-mount and frozen knee sections revealed that at least 60–70% of CXCR6$^+$ cells were costained with the very specific CD1d tetramer that recognizes TCR Vα14*i*, the specific marker for iNKT cells (Fig. 2*A*). Unfortunately, the platelet endothelial cell adhesion molecule-1 (PECAM-1) antibody for mouse endothelium did not work in frozen sections using immunohistochemistry, making it hard to see the vasculature. To determine whether

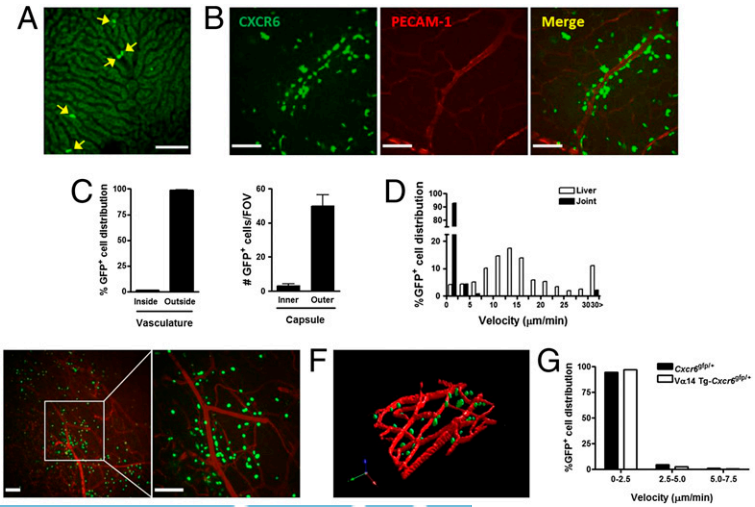

Fig. 1. Extravascular distribution and behavior of iNKT cells in murine joint tissues. Multichannel fluorescent spinning-disk confocal microscopy revealed the knee microvasculature of CXCR6-GFP mice. Representative images showing a characterized distribution of CXCR6$^+$ cells in the liver (*A*) and knee joint tissue (*B*). Most of CXCR6$^+$ cells were localized outside the blood vessel (*C*) and at the extra-articular vasculature of the knee joint ($n \geq 3$ mice per group). (*D*) CXCR6$^+$ cell velocity tracks in the liver and joint microvasculature under normal conditions. Data are representative of more than three independent experiments with more than five fields-of-view (FOVs). (*E*) Representative images from spinning-disk confocal intravital microscopy to visualize iNKT cells in the knee joint tissue of Vα14-Jα18 TCR transgenic (Vα14.Tg) CXCR6-GFP mice at 5–10 min after killing to demonstrate that iNKT cells were the predominant cell type surrounding joint vasculature, and that they were likely there before surgery. Additionally, killing mice allowed for better 3D reconstruction (*F*), highlighting the extravascular distribution of the iNKT cells. (*G*) The majority of Vα14.Tg-CXCR6$^+$ cells were stationary in vivo. Data are representative of more than two experiments. (Scale bars, 100 μm.)

a similar distribution occurred in humans, we first analyzed human synovial biopsies from nonarthritic or mild-arthritic individuals. Consistent with the detection of iNKT cells in mice, double-positive cells for CXCR6 and the invariant CDR3 region of TCR Vα24-Jα18 were found in frozen sections of the anterior compartment or the suprapatellar pouch of the human synovium shown in cross-section (Fig. 2*B*). A cross section reveals that iNKT cells were found outside the vasculature (antibody against human PECAM-1 worked in human frozen sections). However, it is worth noting that there were fewer iNKT cells in human than mouse joints. To explore whether there were any iNKT cells in synovial fluid, a costaining analysis with antibodies against human CD3 and human CD1d-tetramer were used (Fig. 2 *C* and *D*). iNKT cells were barely detectable in the synovial fluid from a patient who has no arthritis (Fig. 2*C*). In contrast, iNKT cells were increased in the synovial fluid from various patients with joint inflammation, including mildly and severely inflamed joints of osteoarthritis (OA) patients, rheumatoid arthritis (RA) patients, and from a patient with Lyme arthritis (Fig. 2*C*). The iNKT cells released into the synovial fluid of arthritis and Lyme disease patients showed higher levels of expression of the activation marker, CD69, than in normal patients (Fig. 2 *D* and *E*). Therefore, iNKT cells are present in human joints and can increase in number and activation status in inflammation.

Immune Surveillance by Extravascular iNKT Cells in Joints. To determine the role of resident iNKT cells in the otherwise normal healthy joint, we focused on a very common infection of joints, namely the Lyme disease-inducing pathogen, *B. burgdorferi*. *B. burgdorferi* expressing the fluorescent protein GFP or Tomato was administered to BALB/c, CXCR6-GFP, or *Cd1d*$^{-/-}$, mice as previously reported (4). *B. burgdorferi* appears as an elongated, highly motile spirochete, often displaying a to-and-fro motion, but when the spirochete dies it becomes a rounded, nonmotile fluorescent particle (confirmed by propidium iodide). Upon intravenous injection, the spirochetes adhere to the inner wall of joint vessels (Fig. 3*A* and Movie S5). iNKT cells in the vicinity of the pathogen and abutting the vessel wall interact with the spirochete. It was not unusual to see the spirochete's tail thrash (Fig. 3*B* and Movie S5). The spirochete did eventually appear outside the vasculature rounded up, nonmotile, and in many cases dead (Fig. 3*C* and Movie S5). These observations suggest that iNKT cells limit the dissemination of *B. burgdorferi* as they exit the vasculature, perhaps through direct killing, although the resolution was not sufficient to conclude direct contact across the vasculature (Fig. 3 *A*–*C*).

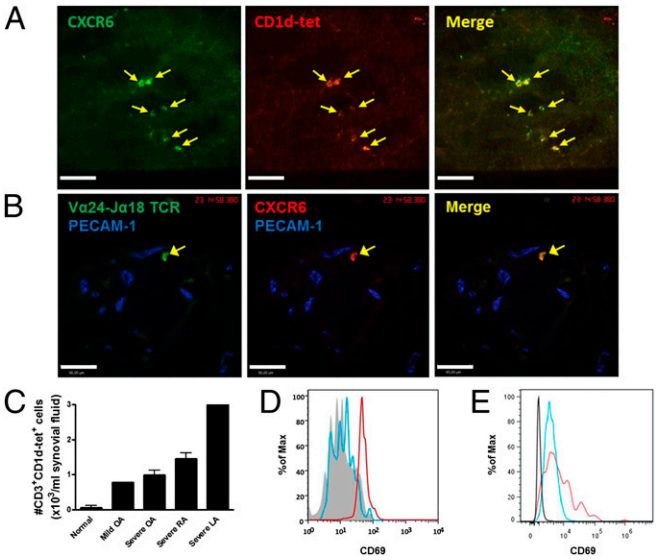

Fig. 2. Detection of iNKT cells in mouse and human knee joint synovium. (*A*) Representative images showing most CXCR6$^+$ cells are CD1d-tetramer$^+$ in the knee joint tissue. Ten-micrometer frozen sections of CXCR6-GFP mouse knee joint were labeled with PBS57-loaded CD1d-tetramer. (*B*) Immunohistochemical analysis of frozen human synovial membrane. Ten-micrometer frozen synovium sections of nonarthritic membrane were labeled with anti-human TCR Vα24-Jα18 (green) and anti-human CXCR6 (red). In *A* and *B*, data are representative of more than two experiments. (*C*) The absolute number of iNKT cells in synovial fluid from normal individuals ($n = 2$) and patients with OA ($n = 1$ for mild; $n = 3$ for severe), RA ($n = 2$), or Lyme arthritis (LA, $n = 1$). Error bars, SEM. The CD69 expression of CD3$^+$CD1-tet$^+$ iNKT cells in peripheral blood (gray) and synovial fluid from mild (blue) and severe (red) OA patients (*D*), and from a Lyme arthritis patient (CD3$^-$CD1-tet$^-$, black; CD3$^+$CD1-tet$^-$, blue; CD3$^+$CD1-tet$^+$, red) (*E*). (Scale bars, 100 μm.)

Increased Bacterial Dissemination in iNKT Cell-Deficient Mice. Spirochetes adhered equally well to the inner vessel wall in wild-type and iNKT cell-deficient (*Cd1d*$^{-/-}$) mice, and the number of adherent *B. burgdorferi* was highest immediately after injection and was progressively reduced over 3 d in wild-type and *Cd1d*$^{-/-}$ mice (Fig. 3*D*). The disappearance of the spirochetes in blood is a result of uptake by macrophage in the liver, as we previously reported (4). As opposed to the liver, where after *B. burgdorferi* infection, intravascular iNKT cells became stationary but did not interact with live *B. burgdorferi* (4), extravascular iNKT cells in the knee changed from being stationary and increased their crawling activity (Fig. 3*E* and Movie S6) and their crawling velocity (Fig. 3*F*), but primarily in areas surrounding where *B. burgdorferi* adhered. In fact, even 100–200 μm away from the adherent pathogen, fewer iNKT cells could be seen crawling and more were adherent (Fig. 3*G*). The increase in crawling behavior was not profound with heat-killed *B. burgdorferi* (Fig. 3*H*). Interestingly, the crawling was not restricted to *B. burgdorferi* but was also seen with *Escherichia coli* (Fig. 3*I*), suggesting perhaps direct detection by one or multiple pathogen-associated molecular patterns, including TLR2 and TLR8 (18, 19), complement, or some other molecule. Indeed, inhibition of complement (Ecb) resulted in decreased iNKT cell crawling behavior after infection (Fig. S1).

The iNKT cells also played a role to limit *B. burgdorferi* in the tissue. It was not unusual to see a *B. burgdorferi* in the extravascular space moving around (Fig. 4*A*, *Left*) until it interacts with an iNKT cell, at which point it remains immobilized for duration of the experiment (Fig. 4*A*, *Right*, and Movie S7). In iNKT-deficient mice, many more *B. burgdorferi* were found moving around the tissues, whereas in wild-type mice, more immobile rounded-up *B. burgdorferi* were detected (Fig. 4*B* and Movie S8). Although the use of Vα14.Tg-CXCR6-GFP mice that only had GFP$^+$ iNKT cells (very few other T cells) showed similar ability to kill *B. burgdorferi* as wild-type mice (Fig. S2), the number of live spirochetes was greatly enhanced in *Cd1d*$^{-/-}$ mice at 3 d after *B. burgdorferi* inoculation (Fig. 4*C*), suggesting a critical role of iNKT cells in bacterial killing as *B. burgdorferi* traverses the vasculature and enters the joint tissue. No heat-killed *B. burgdorferi* were ever found in the knee joint tissue, consistent with an active emigration process by pathogen. We also bred the GFP$^+$ mice with CD1d-deficient mice. These mice still had green fluorescent cells in the joint, but the cells were smaller in appearance than the iNKT cells and we never saw these cells interacting with *B. burgdorferi.* Not surprisingly, these mice also had increased burden of *B. burgdorferi* (Fig. 4*D*). Indeed, in whole iNKT cell-deficient joints, a 25-fold increase in PCR product for *B. burgdorferi* burden have been reported (4, 13), and herein we reveal that the PCR product for *B. burgdorferi* reflects about a fourfold increase in live bacteria living in joint tissue, normally eradicated by iNKT cells.

Granzyme-Dependent Bacterial Killing by Joint iNKT Cells. Recognition of *B. burgdorferi* in liver by iNKT cells required antigen presentation on CD1d via macrophages (4). In striking contrast, blockade of CD1d had no effect on pathogen killing in the knee vasculature (Fig. 5*A*), despite direct intra-articular injection of this antibody, an approach that inhibits function of other cells

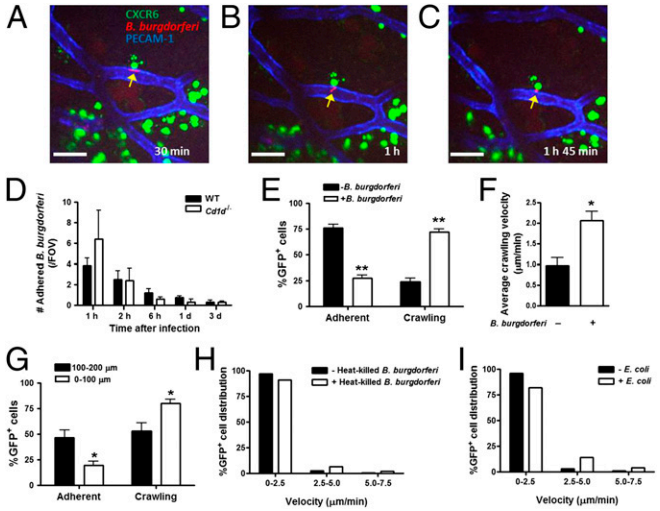

Fig. 3. Extravascular immune surveillance provided by joint iNKT cells in *B. burgdorferi* infection. The knee joint microvasculature of CXCR6-GFP mouse was visualized and recorded for 2.5 h after Tomato-expressing *B. burgdorferi* injection to observe the interaction of iNKT cells, endothelium, and spirochetes. Endothelium was stained with Alexa Fluor 647 anti-mouse PECAM-1. Representative images showing an (*A*) adhering spirochete that (*B*) 30-min later was still alive and appearing to thrash, whereas (*C*) 1 h and 45 min later the spirochete has moved out of the vasculature but is round immobile. A yellow arrow points to the spirochete. (Scale bars, 50 μm.) (*D*) At 1 h, 2 h, 6 h, 1 d, and 3 d after GFP- or Tomato-expressing *B. burgdorferi* injection (intravenous), the number of spirochetes (per FOV) adhered to endothelium was measured in wild-type (BALB/c) or iNKT cell-deficient ($Cd1d^{-/-}$) mouse knee joint vasculature using spinning-disk confocal intravital microscopy ($n \geq 3$ individual mice per group; error bars, SEM). (*E*) Alteration in extracellular iNKT cell behavior after *B. burgdorferi* infection. The number of adherent and crawling iNKT cells at 1–3 h postinfection was compared with noninfection control. (*F*) The average crawling velocity of all cells in the FOV increased. (*G*) Crawling velocity of iNKT cells at 0–100 μm and at 100–200 μm from adhered *B. burgdorferi*. (In *E*–*G*, iNKT cell tracks less than 1 μm/min were considered as adherent; $n \geq 3$ mice per group). Extracelular iNKT cell velocity in response to either (*H*) at 1–3 h after heat-killed *B. burgdorferi* or (*I*) 1–3 h after *E. coli*. Data are representative of two experiments. $^*P < 0.05$ or $^{**}P < 0.01$ vs. noninfected control (–*B. burgdorferi*) by *t* test (in *E* and *F*) and vs. 0–100 μm (in *G*). Error bars, SEM.

using other antibodies. It is worth noting that the iNKT cells could respond to antigen loaded on CD1d to produce IFN-γ (either αGC or *B. burgdorferi*) (Fig. S3). However, this process does not appear to kill *B. burgdorferi* in joints. To determine whether there was direct killing of *B. burgdorferi* by iNKT cells, $CXCR6^+$ cells were isolated from different tissues and coincubated with fluorescent *B. burgdorferi*, and the viability of the spirochetes was determined at 48 h after incubation. Notably, and as illustrated in Fig. 5*B*, coincubation of joint $CXCR6^+$ cells with *B. burgdorferi* resulted in a significant decrease in the number of active bacteria, whereas the cells from liver and spleen were unable to display the lethal activity. In fact, even five-times greater concentrations of $CXCR6^+$ cells from liver and spleen did not show any significant killing activity. It was extremely difficult to get pure iNKT cells from joints because of the limited numbers and additional steps of isolating pure joint iNKT cells. Nevertheless, a few experiments revealed significant killing capacity by purified joint but not liver or spleen iNKT cells (Fig. 5*C*). The reduced killing could be because of reduced function of the iNKT cells as a result of increased isolation steps or another cell type that also helps to kill. Regardless, a pure population of joint iNKT cells can kill *B. burgdorferi*. One difference between liver and joint iNKT cells was predominantly $CD4^+$ iNKT cells in the liver and $CD4^-$ iNKT cells in the joint (Fig. S4).

Previous reports have shown that human iNKT cells do harbor some NK-like cytolytic molecules, including granzyme and perforin (20), and a recent study has identified HOBIT (homolog of Blimp-1 in T cells, Znf683) as a transcriptional program for granzyme in mature iNKT cells that have returned back to thymus but not spleen or liver (7). Therefore, we next investigated how iNKT cells mediate the spirochete cell death and observed a Ca^{2+}-dependent killing mechanism (EGTA inhibitable) (Fig. 5*D*) (21). A serine protease inhibitor 3,4-dichloroisocoumarin (DCI) that blocks granzyme (22), and to a much lesser extent a vacuolar ATPase inhibitor concanamycin A (CMA) that blocks perforin (23), prevented killing of *B. burgdorferi* (Fig. 5*D*). This finding indicated that iNKT cells in joint tissue kill using primarily the granzyme pathway. To further demonstrate this direct killing in vivo via granzyme, mice lacking this molecule also had increased *B. burgdorferi* in joints (Fig. 5*E*). We also stained the iNKT cells from joints and identified very significant increases in granzyme B, but not granzyme A, staining and CD69 activation following *B. burgdorferi* infection (Fig. 5*F* and Fig. S5).

The use of multichannel-fluorescence spinning-disk microscopy in vivo has directly demonstrated the existence of iNKT cells in the joint tissue juxtaposed around microcirculatory vessels and throughout the interstitium, where they play a critical role in limiting *B. burgdorferi* entry into the joint of mice and killing *B. burgdorferi* in the tissue. Although it was well known that iNKT cell-deficient mice have huge *B. burgdorferi* burdens almost exclusively in joints (4), the existence of iNKT cells in joints was previously undetected, perhaps because of their distribution around the sparse vasculature. We also detected

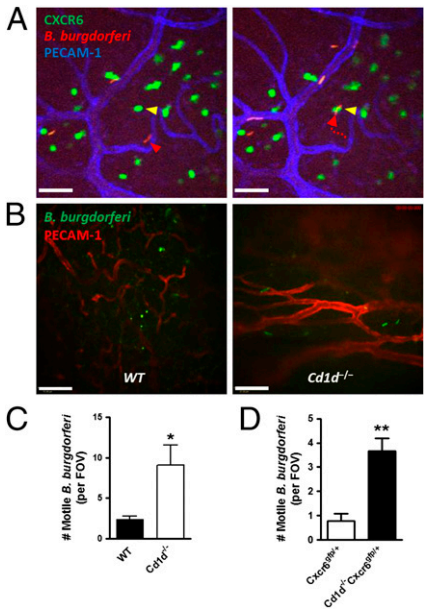

Fig. 4. iNKT cells are critical in the defense against *B. burgdorferi* dissemination into the joint tissue. (*A*) Representative images showing extravasated *B. burgdorferi* in CXCR6-GFP mouse joint at 1 h after infection. (*Left*) Yellow and red arrowheads denote a stationary iNKT cell and a motile *B. burgdorferi* in an extravascular space, respectively. (*Right*) The *B. burgdorferi* is captured by the iNKT cell. A dotted red arrow denotes the crawling route of the *B. burgdorferi*. Captured *B. burgdorferi* remained immobile for duration of the experiment (an additional hour). (Scale bar, 50 μm.) (*B*) Representative images showing that most GFP-expressing particles outside vasculature were round and nonmotile in wild-type knee joint (*Left*) and many intact and motile GFP-expressing spirochetes were infiltrated to outside vasculature at 3 d postinfection in the $Cd1d^{-/-}$ knee joint (*Right*). (Scale bar, 100 μm.) (*C* and *D*) The number of intact/active mobile spirochetes in wild-type (or CXCR6-GFP) and $Cd1d^{-/-}$ (or $Cd1d^{-/-}$CXCR6-GFP) knee joints at 3 d after *B. burgdorferi* infection was measured ($n \geq 3$ mice per group). $^*P < 0.05$, $^{**}P < 0.01$ vs. wild-type (or CXCR6-GFP) by *t* test. Error bars, SEM.

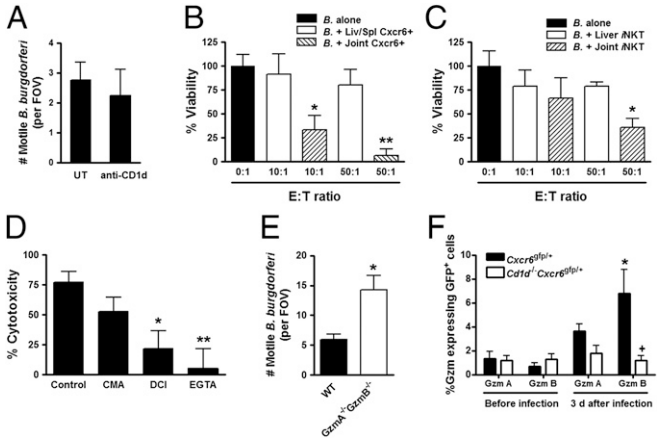

Fig. 5. Direct bactericidal activity provided by joint iNKT cells is granzyme (Gzm)-dependent. (*A*) Effect of anti-CD1d antibody on the clearance of *B. burgdorferi* ("*B.*") spirochetes in knee joint tissue ($n \geq 3$ mice per group). (*B*) Cytotoxic effect of CXCR6$^+$ cells derived from the liver, spleen, or joint tissue on Tomato-expressing *B. burgdorferi*. (*C*) Cytotoxic effect of purified iNKT cells (requiring additional steps) derived from the liver or joint tissue on Tomato-expressing *B. burgdorferi*. (*D*) The effect of CMA, DCI, or EGTA on iNKT cell cytotoxicity. Tomato-expressing *B. burgdorferi* (5×10^3 per milliliter) were incubated with CXCR6$^+$ (*B*) or CXCR6$^+$TCR-β$^+$ (*C* and *D*) cells derived from liver, spleen, or joint at an E:T ratio of 10:1–50:1 at 37 °C and 5% CO_2. The number of surviving *B. burgdorferi* was counted using hemocytometer and spinning-disk confocal microscopy system at 2 d after incubation. CMA, DCI, or EGTA was pretreated with the coculture ($n \geq 5$ FOVs per group). $^{**}P < 0.01$, $^{*}P < 0.05$ vs. target cells alone (*B* and *C*) or vehicle-treated control (*D*) by Bonferroni's multiple-comparison test. Error bars, SEM. (*E*) The number of intact/active mobile spirochetes in wild-type and *Gzma*$^{-/-}$*Gzmb*$^{-/-}$ knee joints at 3 d after *B. burgdorferi* infection was measured ($n \geq 3$ mice per group). $^{*}P < 0.05$ vs. WT by *t* test. Error bars, SEM. (*F*) Gzm expression of GFP$^+$ cells in CXCR6-GFP and *Cd1d*$^{-/-}$CXCR6-GFP mouse joints. Gzm A- or B-expressed cells were analyzed by flow cytometry at 0 d and 3 d after *B. burgdorferi* infection. $^{*}P < 0.05$ vs. before infection, $^{+}P < 0.05$ *vs.* CXCR6-GFP by *t* test. Error bars, SEM.

iNKT cells in human joints, although fewer than seen in mice, perhaps explaining the striking Lyme arthritis in humans but not in infected rodents. Although iNKT cells are visualized in the vasculature of the liver, spleen, and lung (3, 4, 24, 25), a resident blood population of iNKT cells was not observed in the joint vasculature. Moreover, whereas iNKT cells in liver responded to *B. burgdorferi* via CD1d on antigen-presenting cells, inhibition of CD1d had no effect on the host response of iNKT cells in the joints. In fact, unlike iNKT cells in liver, which were unable to recognize live *B. burgdorferi*, joint iNKT cells actively participated in spirochete clearance through a direct bactericidal granzyme-mediated pathway, something neither splenic nor liver iNKT cells could do, even in vitro in direct contact with *B. burgdorferi*. This finding aligns well with the recent publication that a transcription factor BLIMP is turned on in iNKT cells in some tissues but not in the liver or spleen, to allow for the production of granzyme B and other effector mechanisms (7). These differences in iNKT cells in different organs are reminiscent of organ-specific macrophage (Kupffer cells vs. microglia vs. splenic macrophage) and mast cells (mucosal vs. connective tissue).

Using imaging revealed an important barrier function for iNKT cells, and in their absence, *B. burgdorferi* gained easy access into the joint. How the pathogens are recognized by iNKT cells in joints is not clear but we speculate that opsonins, TLRs, or other pattern-recognition molecules may be involved. Indeed, blocking complement reduced the searching/crawling activity of iNKT cells, suggesting opsinization of *B. burgdorferi*, and shed complement fragments must leak into the extravascular space to alert the iNKT cells to the presence of these pathogens (26). Interestingly, we observed similar results after injecting *E. coli*, consistent with broad pathogen-associated molecular pattern detection (such as complement) rather than exclusive CD1d antigen presentation. Clearly, this study highlights the importance of iNKT cell positioning around the vasculature and in the interstitium of the joint, revealing their unique cytolytic activity and raising the possibility that increasing iNKT cell numbers or activity in joint could increase immunity against *B. burgdorferi*.

Materials and Methods

Mice. C57BL/6 (B6), BALB/c, 129X1, *Cd1d*$^{-/-}$, B6.CXCR6-GFP knock-in, Vα14-Jα18 transgenic, and *Gzma*$^{-/-}$*Gzmb*$^{-/-}$ mice were purchased from The Jackson Laboratory. CXCR6-GFP knock-in mice on the BALB/c background were a gift from Dan R. Littman (New York University School of Medicine, New York). *Cd1d*$^{-/-}$CXCR6-GFP mice were made by crossing *Cd1d*$^{-/-}$*Cxcr6*$^{gfp/gfp}$ with *Cd1d*$^{-/-}$*Cxcr6*$^{+/+}$ mice. Mice were maintained in a specific pathogen-free, double-barrier unit at the University of Calgary. All protocols used were in accordance with the guidelines drafted by the University of Calgary Animal Care Committee and the Canadian Council on the Use of Laboratory Animals.

Human Subjects. Patients with OA ($n = 1$, male age: 59 for mild OA; $n = 3$, 2 males age: 35 and 66; 1 female age: 55 for severe OA; Ethics ID #21987) and RA ($n = 2$, females age: 31, 40; Ethics ID #24270) with no other comorbidities consented to arthrocentesis and had synovial fluid aspirated from their knees (volume 5 mL, 20.3 mL ± 6.4 mL and 34.5 mL ± 6.5 mL per recovered knee of mild OA, severe OA, and RA patients, respectively) during a visit to the University of Calgary Foothills Medical Clinic. Synovial fluid from macroscopically normal knees was aspirated from cadavers less than 4 h after death (Ethics ID #21987). Lyme disease patient samples had to be obtained from the Northeast of the United States and were not available in western Canada. Synovial fluid from a Lyme arthritis patient was collected on National Institutes of Health, National Institute of Allergy and Infectious Disease under Institutional Review Board-approved protocol 02-I-0055 ($n = 1$, male age: 65). Synovial fluid from patients treated with any immunosuppressive drugs was excluded.

Intravital Microscopy of the Knee Joint. Murine joint intravital microscopy was performed as previously described (27). Briefly, the jugular vein of the anesthetized mice was cannulated to administer fluorochrome-labeled antibodies and additional anesthetic solution as required. Mice were placed in dorsal recumbency on a heating plate (CU-201, Live Cell Instruments) and body temperature was maintained at 37 °C. The skin and connective tissue over the right knee were surgically removed to expose the anteriomedial aspect of the knee joint and the exposed knee joint was immediately and continuously perfused with warmed buffer (134 mM NaCl, 20 mM $NaHCO_3$, 4.7 mM KCl, 1.2 mM $MgSO_4$, pH 7.4) at a rate of 10 mL/h using a peristaltic pump (Gilson). The mouse was placed on a suitable stage for knee joint intravital microscopy and a glass coverslip was gently placed over the medial aspect of the knee joint with vacuum grease.

Spinning-Disk Confocal Microscopy of the Liver and Knee Joint Tissues. Multichannel fluorescence intravital microscopy of mouse liver and knee joint was done as previously described (4, 27–29). CXCR6-GFP mice were used for the visualization of hepatic and knee joint iNKT cells (3, 4). Anti-mouse PECAM-1 (clone 390; eBioscience) was used for delineation of the joint vasculature. The activity of iNKT cells and bacteria in the knee joint vasculature was assessed simultaneously with three laser-excitation wavelengths in rapid succession (491 nm, 561 nm, and 635 nm; Cobolt) and was visualized with the appropriate band-pass filters (Semrock). Typical exposure time for excitation wavelengths was 0.5–0.7 s. A back-thinned electron-multiplying charge-coupled device camera (C9100-13, Hamamatsu) was used for fluorescence detection. Volocity software (Improvision) was used for acquisition and analysis of images.

Bacterial Strain and Treatment of Mice. The GFP (pTM61) and Tomato (pTM201) expression plasmids were constructed as previously described (28). All *B. burgdorferi* strains were grown for 48 h in BSK-II medium prepared in-house (30) in the presence of 1% (vol/vol) mouse blood (28). For the generation of *B. burgdorferi* strains GCB776 (infectious Tomato), electrocompetent infectious *B. burgdorferi* were prepared from strain B31 5A4 NP1 (31) as previously described (28). The construction of *B. burgdorferi* strain GCB726 (infectious GFP) was also previously reported (28). Mice were intravenously infected via the tail or jugular vein with a dose of 2 or 3×10^8 because it permitted the observation of the interaction of substantial numbers of *B. burgdorferi* in the joint vasculature. For selective blockade of CD1d, 50 μg

anti-mouse CD1d (1B1; eBioscience) was intravenously injected 30 min before and 2 d after *B. burgdorferi* injection (4, 32).

Immunohistochemical Analysis for iNKT Cells. Frozen OCT-embedded knee sections of CXCR6-GFP mice were used for the identification of iNKT cells. For the immunofluorescence analysis, 10-μm tissue sections were obtained and incubated overnight at 4 °C with PE PBS57-loaded murine CD1d-tetramer (National Institutes of Health Tetramer Facility) and Alexa Fluor 647 anti-mouse CD31 (clone 390; BD Pharmigen) at 1:1,000 dilution.

For human studies, knee synovium samples were obtained from patients with no or mild arthritis. These samples were also OCT-embedded and fresh-frozen, and used for the identification of double Vα24-Jα18 TCR and CXCR6 colocalization. Ten-micrometer tissue sections were obtained and incubated overnight at 4 °C with PE anti-human CXCR6 (clone 56811; R&D systems), FITC anti-human TCR Vα24-Jα18 (clone 6B11; BD Pharmigen), and Alexa Fluor 647 anti-human CD31 (clone WM59; BD Pharmigen) at 1:200 dilution. Samples were visualized using a spinning-disk confocal microscope.

Isolation of iNKT Cells and Cytotoxicity Assay. Liver-, spleen-, and joint-derived lymphocytes were isolated from CXCR6-GFP mice using a method previously described (4, 33, 34), with a slight modification. Briefly, livers and spleens were excised and finely minced in a digestive medium containing 0.05% collagenase type IV (Worthington Biomedical) and 0.002% DNase I in HBSS. Joint tissues from mouse hind knees and ankles were placed into Petri dishes containing 5-mL digestion buffer containing 0.1% collagenase type IV, 0.002% DNase I and 5% (vol/vol) FCS. After gentle agitation at 37 °C for 30 min (for liver and spleen) and 2 h (for joint tissues), the concentrate was passed through 100-μm and 40-μm cell strainers. The cell suspension was washed with ice-cold PBS (pH 7.4) and centrifuged at 300 × *g* for 10 min. Mononuclear cells were purified by a 40%/70% (vol/vol) Percoll gradient and were negatively selected with anti-mouse Gr-1 (RB6-8C5; eBioscience), anti-mouse F4/80, anti-mouse CD19 (1D3; eBioscience), and anti-mouse CD8a (53-6.7; eBioscience) microbeads and MACS column to remove neutrophils, macrophages, B cells, and $CD8a^+$ cells, respectively. $CXCR6\text{-}GFP^+$ or $TCR\text{-}\beta^+GFP^+$ (iNKT) cells from 5 to 6 mice were sorted. $CXCR6\text{-}GFP^+$ cells or iNKT cells were resuspended in RPMI medium containing 20% (vol/vol) FCS, 100 U/mL penicillin, and 100 μg/mL streptomycin.

Tomato-expressing *B. burgdorferi* (GCB776, 5×10^3 cells/mL) were incubated with $CXCR6^+$ cells or iNKT cells at an effector cell:target cell (E:T) ratio of 10:1–50:1 at 37 °C and 5% CO_2. Because the *B. burgdorferi* strain used is streptomycin- and penicillin-sensitive, but gentamicin-insensitive, the cells were incubated in RPMI medium containing 20% (vol/vol) FCS and 50 μg/mL gentamicin. The cells were placed in a 96-well U-shape bottom culture plate for the experiment. The viability of *B. burgdorferi* was not altered at least for 48 h. For some experiments, iNKT cells were treated with 10 nM CMA (Sigma-Aldrich), 50 μM DCI (Sigma-Aldrich), or 2 mM EGTA (Sigma-Aldrich). The number of *B. burgdorferi* survived per well was determined at 48 h after incubation using hemocytometer and spinning-disk confocal fluorescent microscopy. The inhibitory effect derived by CMA, DCI, and EGTA was standardized by inhibitor alone group (without iNKT cells).

Flow Cytometry for Human Synovial Fluid. Synovial fluids from patients with no, mild, or severe arthritis were washed with cold PBS and centrifuged at 50 × *g* for 20 min at 4 °C. The resuspended cells were filtered by a 100-μm cell strainer. Cells were incubated with PerCP-Cy5.5 anti-human CD3 (clone OKT3, eBioscience), PE anti-human PBS57-loaded human CD1d tetramer (National Institutes of Health) and FITC anti-human CD69 (clone FN50; eBioscience). All samples were analyzed on an Attune acoustic focusing cytometer (Applied Biosystems) or BD FACScan system (BD Biosciences).

Statistical Analyses. All values were expressed as mean ± SEM. Data were compared either by unpaired two-tailed Student *t* test or one-way ANOVA with Bonferroni multiple comparisons post hoc test. Statistical significance was accepted at $P < 0.05$.

ACKNOWLEDGMENTS. We thank the Live Cell Imaging Facility for training/assistance related to microscopy (P. Colarusso and K. Stevens); the Flow Cytometry Facility for their assistance (L. Kennedy and Y. Liu); and T. Nussbaumer for excellent technical support. Work in the authors' laboratory is supported by Canadian Institutes for Health Research operating grants and group grant, as well as the Canadian Foundation for Innovation; P.K. is an Alberta Innovates Health Solutions Scientist and the Snyder Chair in Critical Care Medicine; M.-J.S. is supported by a grant from the Spanish Ministry of Education (PR2010-0477); G.C. received salary support as the Canada Research Chair in the Molecular Biology of Lyme borreliosis and in the form of a Scientist Award from the Alberta Heritage Foundation for Medical Research, as well as operating grant support from the Canadian Institutes of Health Research (MOP-53086).

1. Hickey MJ, Kubes P (2009) Intravascular immunity: The host-pathogen encounter in blood vessels. *Nat Rev Immunol* 9(5):364–375.
2. Auffray C, et al. (2007) Monitoring of blood vessels and tissues by a population of monocytes with patrolling behavior. *Science* 317(5838):666–670.
3. Geissmann F, et al. (2005) Intravascular immune surveillance by $CXCR6^+$ NKT cells patrolling liver sinusoids. *PLoS Biol* 3(4):e113.
4. Lee W-Y, et al. (2010) An intravascular immune response to *Borrelia burgdorferi* involves Kupffer cells and iNKT cells. *Nat Immunol* 11(4):295–302.
5. Bendelac A, Savage PB, Teyton L (2007) The biology of NKT cells. *Annu Rev Immunol* 25:297–336.
6. Kronenberg M (2005) Toward an understanding of NKT cell biology: Progress and paradoxes. *Annu Rev Immunol* 23:877–900.
7. van Gisbergen KP, et al. (2012) Mouse Hobit is a homolog of the transcriptional repressor Blimp-1 that regulates NKT cell effector differentiation. *Nat Immunol* 13(9):864–871.
8. Kawano T, et al. (1997) CD1d-restricted and TCR-mediated activation of valpha14 NKT cells by glycosylceramides. *Science* 278(5343):1626–1629.
9. Brossay L, et al. (1998) CD1d-mediated recognition of an alpha-galactosylceramide by natural killer T cells is highly conserved through mammalian evolution. *J Exp Med* 188(8):1521–1528.
10. Kobayashi E, Motoki K, Uchida T, Fukushima H, Koezuka Y (1995) KRN7000, a novel immunomodulator, and its antitumor activities. *Oncol Res* 7(10-11):529–534.
11. Mattner J, et al. (2005) Exogenous and endogenous glycolipid antigens activate NKT cells during microbial infections. *Nature* 434(7032):525–529.
12. Kinjo Y, et al. (2006) Natural killer T cells recognize diacylglycerol antigens from pathogenic bacteria. *Nat Immunol* 7(9):978–986.
13. Tupin E, et al. (2008) NKT cells prevent chronic joint inflammation after infection with *Borrelia burgdorferi*. *Proc Natl Acad Sci USA* 105(50):19863–19868.
14. Steere AC (2001) Lyme disease. *N Engl J Med* 345(2):115–125.
15. Steere AC, Schoen RT, Taylor E (1987) The clinical evolution of Lyme arthritis. *Ann Intern Med* 107(5):725–731.
16. Matsuda JL, et al. (2000) Tracking the response of natural killer T cells to a glycolipid antigen using CD1d tetramers. *J Exp Med* 192(5):741–754.
17. Katchar K, Drouin EE, Steere AC (2013) Natural killer cells and natural killer T cells in Lyme arthritis. *Arthritis Res Ther* 15(6):R183.
18. Cervantes JL, et al. (2011) Phagosomal signaling by *Borrelia burgdorferi* in human monocytes involves Toll-like receptor (TLR) 2 and TLR8 cooperativity and TLR8-mediated induction of IFN-beta. *Proc Natl Acad Sci USA* 108(9):3683–3688.
19. Oosting M, et al. (2011) TLR1/TLR2 heterodimers play an important role in the recognition of *Borrelia* spirochetes. *PLoS ONE* 6(10):e25998.
20. Kuylenstierna C, et al. (2011) NKG2D performs two functions in invariant NKT cells: direct TCR-independent activation of NK-like cytolysis and co-stimulation of activation by CD1d. *Eur J Immunol* 41(7):1913–1923.
21. Veugelers K, et al. (2006) Granule-mediated killing by granzyme B and perforin requires a mannose 6-phosphate receptor and is augmented by cell surface heparan sulfate. *Mol Biol Cell* 17(2):623–633.
22. Baba T, et al. (2008) Rat $CD4^+CD8^+$ macrophages kill tumor cells through an NKG2D- and granzyme/perforin-dependent mechanism. *J Immunol* 180(5):2999–3006.
23. Ma LL, et al. (2004) NK cells use perforin rather than granulysin for anticryptococcal activity. *J Immunol* 173(5):3357–3365.
24. Scanlon ST, et al. (2011) Airborne lipid antigens mobilize resident intravascular NKT cells to induce allergic airway inflammation. *J Exp Med* 208(10):2113–2124.
25. Barral P, Sánchez-Niño MD, van Rooijen N, Cerundolo V, Batista FD (2012) The location of splenic NKT cells favours their rapid activation by blood-borne antigen. *EMBO J* 31(10):2378–2390.
26. Hawley KL, et al. (2012) CD14 cooperates with complement receptor 3 to mediate MyD88-independent phagocytosis of *Borrelia burgdorferi*. *Proc Natl Acad Sci USA* 109(4):1228–1232.
27. Andruski B, McCafferty DM, Ignacy T, Millen B, McDougall JJ (2008) Leukocyte trafficking and pain behavioral responses to a hydrogen sulfide donor in acute monoarthritis. *Am J Physiol Regul Integr Comp Physiol* 295(3):R814–R820.
28. Moriarty TJ, et al. (2008) Real-time high resolution 3D imaging of the Lyme disease spirochete adhering to and escaping from the vasculature of a living host. *PLoS Pathog* 4(6):e1000090.
29. Norman MU, Hulliger S, Colarusso P, Kubes P (2008) Multichannel fluorescence spinning disk microscopy reveals early endogenous CD4 T cell recruitment in contact sensitivity via complement. *J Immunol* 180(1):510–521.
30. Barbour AG (1984) Isolation and cultivation of Lyme disease spirochetes. *Yale J Biol Med* 57(4):521–525.
31. Kawabata H, Norris SJ, Watanabe H (2004) BBE02 disruption mutants of *Borrelia burgdorferi* B31 have a highly transformable, infectious phenotype. *Infect Immun* 72(12):7147–7154.
32. Faunce DE, Palmer JL, Paskowicz KK, Witte PL, Kovacs EJ (2005) CD1d-restricted NKT cells contribute to the age-associated decline of T cell immunity. *J Immunol* 175(5):3102–3109.
33. Ajuebor MN, Hogaboam CM, Le T, Swain MG (2003) C-C chemokine ligand 2/monocyte chemoattractant protein-1 directly inhibits NKT cell IL-4 production and is hepatoprotective in T cell-mediated hepatitis in the mouse. *J Immunol* 170(10):5252–5259.
34. Sonderegger FL, et al. (2012) Localized production of IL-10 suppresses early inflammatory cell infiltration and subsequent development of IFN-γ-mediated Lyme arthritis. *J Immunol* 188(3):1381–1393.